Numerical and experimental investigation of FDM fabricated re-entrant auxetic structures of ABS and PLA materials under compressive loading

Swapnil Vyavahare and Shailendra Kumar
Department of Mechanical Engineering, Sardar Vallabhbhai National Institute of Technology, Surat, India

Abstract

Purpose – Auxetic structures are one type of mechanical meta-materials mainly used for energy absorption applications because of their unique negative Poisson's ratio. This study is focused on numerical and experimental investigations of fused deposition modeling (FDM) fabricated re-entrant auxetic structures of acrylonitrile butadiene styrene (ABS) and poly-lactic acid (PLA) materials under compressive loading. Influence of geometric parameters, namely, re-entrant angle, height and arm-length on strength, stiffness and specific energy absorption (SEA) of auxetic structures under compressive loading. Optimization of significant parameters is also performed to maximize these responses and minimize weight and time of fabrication. Further, efforts have also been made to develop predictive models for strength, stiffness and SEA of auxetic structures.

Design/methodology/approach – A full factorial design of experiment is used for planning experiments. Auxetic structures of ABS and PLA are fabricated by FDM technique of additive manufacturing within the constrained range of geometric parameters. Analysis of variance is performed to identify the influence of geometric parameters on responses. To optimize the geometric parameters Gray relational analysis is used. Deformation of auxetic structures is studied under compressive loading. A numerical investigation is also performed by building nonlinear finite element models of auxetic structures.

Findings – From the analysis of results, it is found that re-entrant angle, height and arm-length with their interactions are significant parameters influencing responses, namely, strength, stiffness and SEA of the auxetic structures of ABS and PLA materials. Based on the analysis, statistical nonlinear quadratic models are developed to predict these responses. Optimal configurations of auxetic structure of ABS and PLA are determined to maximize strength, stiffness, SEA and minimize weight and time of fabrication. From the study of deformation of auxetic structures, it is found that ABS structures have higher energy absorption, whereas PLA structures have better stiffness. Results of finite element analysis (FEA) are found in good agreement with experimental results.

Research limitations/implications – The present study is limited to re-entrant type of auxetic structures of ABS and PLA materials only under compressive loading. Also, results from the present study are valid within the selected range of geometric parameters. The findings of the present study are useful in maximizing strength, stiffness and SEA of auxetic structures that have wide applications in the automotive, aerospace, sports and marine sector.

Originality/value – No literature is available on studying the influence of geometric parameters, namely, re-entrant angle, height and arm-length of auxetic structure on strength, stiffness and SEA under compressive loading. Also, a comparative study of feedstock materials, namely, ABS and PLA, is also not reported. The present work attempts to fulfill the above research gaps.

Keywords Fused deposition modeling, Additive manufacturing, Compressive loading, Geometric parameter, Re-entrant auxetic structure

Paper type Research paper

1. Introduction

Lightweight structures that satisfy strength, stiffness and energy absorption criteria are the prevailing topic in the current customer-centric product development environment. With recent development in additive manufacturing (AM) processes, tailor-made shapes and sizes are possible for complex structures. Meta-materials are human made structures having counterintuitive properties developed because of their geometry. Because of the unique capability of regulation of properties (strength, stiffness and energy absorption), these materials have gained attention in recent times in various fields (Yu *et al.*, 2018). These structures have unique mechanical properties such as negative Poisson's ratio (NPR), less shear modulus, negative compressibility and negative stiffness, which differentiate them from conventional structures. Among these meta-materials, NPR structures have unique mechanical properties like high strength to weight ratio, indentation resistance, impact resistance, bending stiffness, fracture toughness, vibration damping, hardness and excellent shock

The current issue and full text archive of this journal is available on Emerald Insight at: **https://www.emerald.com/insight/1355-2546.htm**

Rapid Prototyping Journal

[DOI 10.1108/RPJ-10-2019-0271]

Received 29 April 2020
Revised 10 July 2020
Accepted 24 August 2020

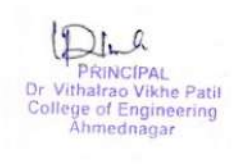

absorption capacity as compared to the conventional positive Poisson's ratio structures (Elipe and Lantada, 2012; Zhang and Yang, 2016). NPR structures (or auxetic structures) are classified based upon the geometry of unit cells such as re-entrant, chiral, star-shaped, rota-chiral, lozenge, etc. Mechanical properties of these structures can be improved by optimizing geometric parameters under different loading conditions such as compression, shear, flexural, impact, etc. Under compression loading, auxetic structure has better energy absorption capability than the conventional honeycomb structure (Ingrole *et al.*, 2017). Re-entrant type auxetic structure has better mechanical properties than other NPR structures (Elipe and Lantada, 2012; Yang *et al.*, 2015). Re-entrant angle (θ), height (h), arm-length (l) and thickness of strut (t) are major geometric parameters of the unit cell of a re-entrant auxetic structure as shown in Figure 1. Properties of re-entrant auxetic structure are influenced by these geometric parameters (Scarpa, 2000; Panda *et al.*, 2018). To manufacture re-entrant auxetic structures, conventional manufacturing is not suitable, as it requires specific tooling which increases cost and time of fabrication. Thus, in such a scenario AM is used to fabricate these complex structures. Fused deposition modeling (FDM) is one of the techniques of AM, in which there is layer-by-layer material addition in semisolid form. It is the most popular AM technique because it is economical and capable of fabricating parts of variety of polymeric materials. Nowadays, FDM is not only used for prototyping but also used for the manufacturing of functional parts (Lam *et al.*, 2002; Negis, 2009; Korpela *et al.*, 2013; Okwuosa *et al.*, 2016; Bayar and Aziz, 2018). Low-density lightweight structures fabricated by FDM have wide applications in automotive, aerospace, sports and marine sector (Durgun, 2015; Meier *et al.*, 2018; Garcia-Garcia and Gonzalez-Palacios, 2018).

Many researches have made efforts to investigate different structures fabricated by FDM and developed predictive models by analytical, numerical and experimental techniques. Zhang and Yang (2016) performed a parametric analysis of the effect of Poisson's ratio (cell angle) and relative density (wall thickness) on mechanical properties of auxetic structures. They concluded that the ultimate strength of structure is scale dependent when Poisson's ratio and relative density is kept constant. Ingrole *et al.* (2017) developed a hybrid structure by combining regular and auxetic structures. They further improved this structure by introducing a strut in the auxetic region of the structure. Xu *et al.* (2018) studied the effect of microstructure and tube alignment on out-of-plane compressive properties of honey tubes. They observed higher energy absorbing capacity and local strain in tubes and tube-rib connection as compared to conventional honeycomb

Figure 1 Re-entrant auxetic unit cell showing geometric parameter

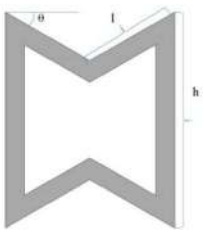

structure. Chen *et al.* (2018) described the in-plane compressive performance of hierarchical cellular structure. They further applied thermal treatment to facilitate shape preservation under large compressive loading. Thus structure's stiffness and energy absorption capacity increased. Li *et al.* (2018a) investigated on off-axis compressive loading of square honeycombs. They found that the in-plane strength of square honeycomb depends on in-plane off-axis angles. These square honeycombs exhibit a high yield strength in principal direction than in-plane off-axis direction. Yang *et al.* (2018) have made efforts in studying various types of structures of different materials. The shock-absorbing performance of auxetic structure was found better than the regular honeycomb. Panda *et al.* (2018) conducted an experimental study to investigate the effect of geometric parameters on mechanical properties. They developed various models by genetic programming (GP), automated neural network (ANN), fuzzy logic and response surface methodology (RSM) and compared their performances with experimental findings. It was found that ANN models perform best, followed by GP and RSM. Raeisi *et al.* (2019) compared the compressive performance of regular, auxetic and hybrid honeycomb structures. These structures were compared for mechanical properties with the same relative density. Hybrid structure developed by the combination of design of regular and auxetic honeycomb structures exhibited the best performance. Xu *et al.* (2019) derived the relationship of mechanical properties along different loading directions of Aux-Hex structure. In *X*-direction, energy absorption capacity was increased by 38% with uniform and stable deformation of unit cells. Li *et al.* (2019) studied the compressive behavior of auxetic reinforced honeycomb. It was observed that auxetic lattice reinforced composite had better mechanical performance as compared to non-auxetic. Alomarah *et al.* (2020a) performed a comparative study of re-entrant chiral (RCA) and regular re-entrant structure experimentally and numerically under compression loading. Multi-jet fusion technique with a polyamide 12 (PA12) was used for specimen fabrication. It is found that RCA structure outperforms regular auxetic structure for strength and specific energy absorption (SEA). McCaw and Cuan-Urquizo (2020) validated a mathematical approach to parameterize lattices into Bezier surfaces and also fabricated non-planer lattices via curved-layer fused deposition. Geometrical parameters of lattice were varied and specimens were tested under cyclic loading. They observed that lattices with higher auxeticity result in less energy dissipation. Attard *et al.* (2020) studied star-chiral auxetic structure numerically and experimentally. The hierarchical deformation mechanism was observed by varying geometrical parameters of unit cell of structure. It was found that Poisson's ratio is dependent on the ratio of thickness and ration of ligaments. Gao *et al.* (2020) established theoretical nonlinear models of 2-dimensional (2D) and 3-dimensional (3D) Double-V micro-structure to anticipate normalized Young's modulus and Poisson's ratio as a function of strain. A significant effect of geometrical parameters was observed on these mechanical properties. A summary of major research work in the domain of mechanical properties' evaluation of different structures is given in Table 1.

Table 1 Summary of major research in mechanical property evaluation of structures

Researchers	Structures	Loading	Method used	Properties investigated
Zhang and Yang (2016)	Auxetic	In-plane compressive and dynamic	Numerical and experimental	Strength and dynamic performance
Ingrole *et al.* (2017)	Hexagonal, auxetic and hybrid	In-plane compressive	Experimental and numerical	Yield strength, stiffness
Chen *et al.* (2018)	Hierarchical cellular	In-plane large compressive and cyclic	Numerical and experimental	Stiffness and energy absorption
Li *et al.* (2018a)	Square	Off-axis in-plane compressive	Theoretical, numerical and experimental	Yield strength
Panda *et al.* (2018)	Hexagonal	Out-plane compressive	Experimental and computational intelligence	Yield strength, stiffness
Raeisi *et al.* (2019)	Hexagonal, auxetic, hybrid	In-plane compressive	Numerical and experimental	Yield strength, stiffness
Xu *et al.* (2018)	Hollow lattice truss reinforced honecomb	Out-plane compressive	Experimental and numerical	Yield strength, stiffness
Xu *et al.* (2019)	AuxHex	In-plane compressive	Theoretical, numerical and experimental	Stiffness, plastic collapse stress and energy absorbing capacity
Yang *et al.* (2018)	Auxetic (Re-entrant and arrowhead)	In-plane compressive and impact	Theoretical, numerical and experimental	Stiffness and shock absorption performance
Li *et al.* (2019)	Auxetic	In-plane compressive	Numerical and experimental	Stiffness and energy absorption
Alomarah *et al.* (2020a)	Re-entrant chiral (RCA) and regular re-entrant structure	In-plane compressive	Numerical and experimental	Strength and specific energy absorption
McCaw and Cuan-Urquizo (2020)	Lattices	Cyclic-loading	Theoretical and experimental	Auxeticity
Attard *et al.* (2020)	Star-chiral auxetic structure	In-plane compressive	Numerical and experimental	Poisson's ratio
Gao *et al.* (2020)	Double-V micro-structure	In-plane compressive	Theoretical, numerical and experimental	Normalized Young's modulus and Poisson's ratio

The previously mentioned literature review reveals that limited efforts are made to investigate the influence of geometric parameters on mechanical properties of auxetic structures of different materials. In the present work, efforts are made to investigate the properties of FDM fabricated auxetic structures of acrylonitrile butadiene styrene (ABS) and poly-lactic acid (PLA) materials. Both the materials are supplied by M/s Positron Additive Ltd., Pune, India in the form of filament (diameter – $1.75^{\pm 0.03}$ mm). Objectives of the present study are following:

- to study the influence of geometric parameters on strength, stiffness and SEA of FDM fabricated re-entrant auxetic structures under compressive loading;
- to optimize significant geometric parameters to maximize strength, stiffness and SEA; and minimize weight and time of fabrication of structures;
- to develop regression models for strength, stiffness and SEA; and
- to study deformation of auxetic structures experimentally and numerically.

2. Experimental details

In the present study, experimentation involves the following steps:

- experimental design;
- Computer-aided design (CAD);
- fabrication of parts using FDM;
- finite element analysis (FEA); and
- measurement of responses of auxetic structures.

2.1 Experimental design

Three geometric parameters of the auxetic structure, namely, re-entrant angle, height and arm-length are considered in the present study. Levels of these parameters as given in Table 2 are decided based on literature review. A comprehensive experimental study is planned using a full factorial design with the help of Design-Expert 11 software (developed by Stat-Ease Inc.). As given in Table 3, experimental design suggested a total of 16 experiments for each material (i.e. ABS and PLA). The thickness of cell wall of the auxetic structure is calculated for constant relative density by rearranging the terms in equation (1) (Gibson and Ashby, 1999; Raeisi *et al.*, 2019). In a linear elastic regime, apparent Young's modulus of the meta-material sample is related to relative density as given by equation (2) (Surjadi *et al.*, 2019). Figure 2 shows the auxetic cellular structure with vertical and inclined walls. In-plane properties are related to loads applied in the *X*-*Y* plane and out-of-plane properties are a response to loads applied to the faces normal to *Z*-direction. Table 4 lists values of thickness (t) calculated using equation (1) for all configurations by keeping relative density as 35%. In the present study, the number of unit cell repetitions is 9 (3×3); therefore, the size effect of the structure is neglected as the number of unit cell repetitions is more than 3 (Alomarah *et al.*, 2018).

Table 2 Geometric parameters and their range

Geometrical parameters		Range
Re-entrant angle (A) (degree)	20	40
Height (B) (mm)	14	18
Arm length (C) (mm)	5	8

Table 3 Experimental design

Run no.	Re-entrant angle Degree	Height mm	Arm length mm
1	40	18	5
2	20	14	5
3	40	14	8
4	20	18	5
5	20	14	8
6	20	18	5
7	40	14	5
8	20	18	8
9	40	18	5
10	40	18	8
11	40	18	8
12	40	14	8
13	40	14	5
14	20	14	5
15	20	14	8
16	20	18	8

Figure 2 Auxetic cellular structure

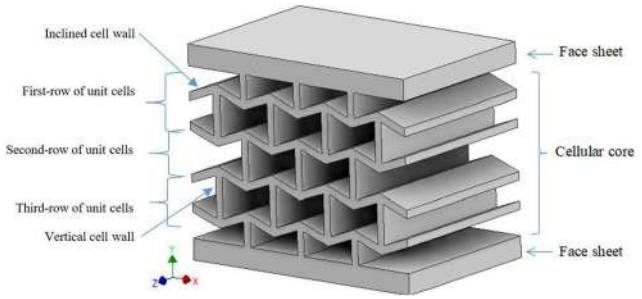

$$\left(\frac{\rho*}{\rho s}\right) = \frac{\left(\frac{t}{l}\right) \times \left(\left(\frac{h}{l}\right) + 2\right)}{2 * \cos\theta \times \left(\left(\frac{h}{l}\right) + \sin\theta\right)} \qquad \text{equation (1)}$$

where,

$\rho^\star$ = density of auxetic structure;
ρ_s = density of solid material from which struts are made;
$\rho^\star/\rho_s$ = relative density of auxetic structure;t= thickness of strut;
θ = angle of the strut with respect to the horizontal axis;h = height of auxetic structure; and
l = arm-length of auxetic structure.

$$\frac{E}{Es} \approx \left(\frac{\rho}{\rho s}\right)^2 \qquad \text{equation (2)}$$

where
E = Young's modulus of cellular architecture; and
Es = Young's modulus of constituent solid material.

2.2 Computer-aided design

As per the experimental design, eight different configurations are modeled. Unit cells of each type of configuration are modeled in Autodesk Inventor 2020 software and then arrayed in the *XY* plane and extruded along *Z*-direction. To avoid out-of-plane buckling and to focus on 2D in-plane compressive loading, the thickness of the sandwich structure is chosen as 40 mm (Ingrole *et al.*, 2017). The thickness of the upper and lower face sheet is 5 mm for all configurations. The representative CAD model of the specimen is shown in Figure 2. All geometrical files are saved in standard tessellation language (STL) format.

2.3 Specimen fabrication

STL files of modeled structures are imported in CURA 4.2.1 software. GCODE files are prepared and then fed to the FDM machine one-by-one to fabricate specimens. The FDM machine used (Model: Delta 2040, M/s. WASP, Italy) in the present work is provided with a nozzle of 0.4 mm diameter. In the present work for the fabrication of structures, layer thickness is kept constant as 0.2 mm. The print temperatures are taken as 240°C and 210°C, and bed temperatures are 100° C and 60°C for ABS and PLA material, respectively. Infill percentage is kept as 100% with inner and outer wall speed as 60 mm/s and 30 mm/s, respectively. Figure 3 shows the number of contours and raster angle orientation for auxetic structure. The number of contours for each cell wall is two as the minimum cell wall thickness of 1.205 mm (for Configuration 5) and the raster width is 0.3 mm. For other configurations, the cross-section area is filled by additional rasters at 90°. Specimens are manufactured along *Z*-direction as shown in Figure 2 to avoid the use of supports and the impact of build orientation on mechanical properties. Also, *Z*-axis as a build orientation and *Y*-axis as loading direction produces components with maximum strength as the load is carried axially along fibers (Ahn *et al.*, 2002). Time for fabrication for

Table 4 Geometric parameters and their values

Configuration no.	Re-entrant angle (°)	Height (mm)	Arm length (mm)	Thickness of cell wall (mm)	Run no.
1	20	14	5	1.700	2,14
2	20	14	8	2.000	5,15
3	40	14	8	1.3	3,12
4	20	18	5	1.9	4,6
5	40	14	5	1.205	7,13
6	40	18	8	1.65	10,11
7	20	18	8	2.38	8,16
8	40	18	5	1.42	1,9

Figure 3 Number of contours and raster angle orientation for configuration no. 5 auxetic structure

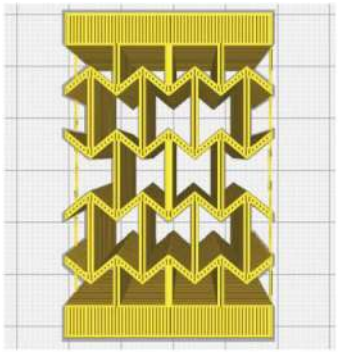

each configuration is noted using a stopwatch. The weight of structures is measured using a digital scale.

Quasi-two-dimensional specimens are created with the same number of unit cells (3×3), which gives cellular structure with an approximate size of $50 \times 40 \times 40\text{mm}^3$. Two structures of both materials are fabricated for each configuration to minimize experimental error. Thus total 32 structures are fabricated, as shown in Figure 4(a) (PLA structures are in black color while ABS structures are in white color). Figure 4(b) shows configuration number 8 auxetic sandwich core structure of ABS material.

2.4 Finite element analysis

Material properties of structures fabricated by FDM are different from the properties of filament because of build-orientation selected for fabrication and anisotropic nature of the FDM process. Therefore, two specimens of size ϕ 12.5×25.4 mm of each material (i.e. ABS and PLA) are fabricated as shown in Figure 5 according to the build orientation of auxetic structures (axis of cylinder parallel to *XY*-plane) (Ahn *et al.*, 2002). Same values of process parameters are used in fabrication of cylindrical specimen as used in auxetic structures. Quasi-static compressive loading of these specimens is performed in *Y*-direction in accordance with ASTM D695. The stress is computed as a ratio of measured force over the original cross-sectional area. The strain is computed as the ratio of displacement over the original gauge length. Resultant material properties are listed in Table 5, which are used in the FEA of auxetic structures. Values of Poisson's ratio are taken from the literature (Ingrole *et al.*, 2017; Araujo *et al.*, 2019).

Figure 4 (a) Fabricated auxetic structures and (b) configuration No. 8 of ABS material

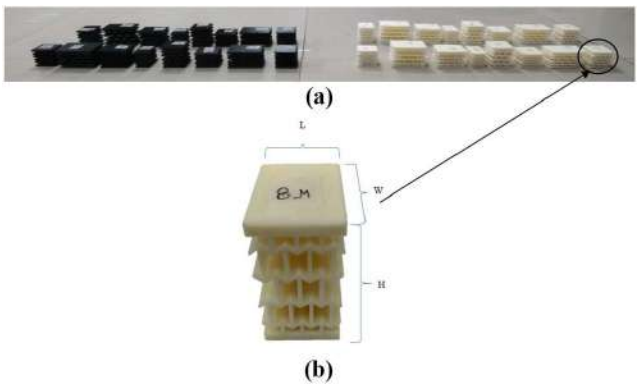

A series of 3 D finite element (FE) models are developed according to each geometrical configuration of auxetic structure using ABAQUS/Standard solver. FE models are developed with an assumption of plain strain type. A fixed constraint is given to the bottom surface of structures and movement is given to the top surface. The eight node SOLID elements with reduced integration and hourglass control (C3D8R) are used in the analysis of all configurations to get high accuracy with minimum analysis time (Araújo *et al.*, 2019; Francesconi *et al.*, 2019a; Francesconi *et al.*, 2019b; Lee *et al.*, 2019; Li *et al.*, 2018b; Li *et al.*, 2019; Al-Rifaie and Sumelka, 2019; Saxena *et al.*, 2017; Wang *et al.*, 2019; Xu *et al.*, 2018). Geometric and material nonlinearity is taken into attention to have large deformation. Mesh control used is the hex-dominant element shape with sweep technique and advancing front algorithm. In addition, for FE models, general contact is used to simulate contact interaction between surfaces of models to avoid interpenetration of unit cells during analysis. Interaction property for contact is used as "ALL WITH SELF" along with tangential behavior, penalty as friction formulation, and 0.2 as friction coefficient (μ). The load-displacement curve and values of initial stiffness, energy absorbed and maximum stress are obtained from simulation. The strength of each configuration is evaluated from maximum stress.

2.5 Measurement of responses of auxetic structures

Quasi-static uniaxial compressive tests are performed on a universal testing machine (Universal testing machine (UTM), FSA Model – TUE-C) at a crosshead speed of 5 mm/min. Load-displacement curves, initial stiffness, energy absorbed are assessed. Failure mechanisms of specimens are evaluated. The applied force is measured by the machine load cell. Tests are conducted according to ASTM C365, which is a standard test method for flat-wise compression properties of sandwich cores (Scarpa *et al.*, 2007; Xu *et al.*, 2018). Displacement is measured with a mechanical extensometer in-built in UTM. Two specimens are tested for each configuration of the structure. The load-displacement curves measured from the uniaxial compression test are converted in the stress–strain curves by measuring dimensions of the specimens. Stiffness is calculated from the initial linear region of the stress–strain curve. Structures are tested until 60% strain. A video camera is positioned on one side of the specimen to capture the row-by-row deformation of structure. Nominal stress and strain are computed according to dimensions of the structure as shown in Figure 4(b). Deformation of all configurations at nominal strain (ε) of 0.15 and stress-strain curves is given in Appendix 1 and 2, respectively.

3. Results and discussion

Experimental results for fabricated auxetic structures of ABS and PLA materials are given in Table 6. The experimental results are

Figure 5 Specimen for compressive testing

Notes: (a) CAD model; (b) fabricated ABS specimen; (c) fabricated PLA specimen

Table 5 Material properties of ABS and PLA

Material	Density, ρ (gm/cm^3)	Modulus of elasticity, E (GPa)	Poisson' ratio, ν	Yield strength, σ_y (MPa)
ABS	1.05	2.2	0.35	31
PLA	1.252	3.5	0.36	20

evaluated by using Design-expert 11 software. From the stress–strain curve of all configurations, it is clear that structures initially resist load and then the cell wall starts collapsing. Once collapsed cells become compacted, structures start resisting load again. The increase and decrease in stress continue until the whole structure is compacted. This deformation behavior is observed in all configurations with slight variation as per the geometry of unit cell and material of the structure. As depicted in Figure 6 stress–strain curve of each configuration displays similar deformation behavior with three distinct deformation stages, namely, linear-elastic stage, plateau stage and densification stage. The unit cell undergoes elastic deformation mode followed by plateau stress with an increase in strain. Within this strain-range, strictures undergo elastic–plastic deformation because of the bending of inclined cell walls. Further increase in strain leads to the initial failure of cell walls. With a small value of strain, stress–strain curves look almost linear and accordingly stiffness is calculated. Once structure reaches the critical limit of strain, failure occurs owing to buckling/brittle fracture depending upon the material. On increasing load, opposite cell walls come in contact with each other which results in collapsing of cell walls. It is the start of the densification stage which increases the stiffness of the structure.

Table 6 Experimental results for auxetic structures

Material	ABS			PLA		
Run no.	Compressive strength MPa	Compressive modulus MPa	SEA J/gm	Compressive strength MPa	Compressive modulus MPa	SEA J/gm
1	2.586	85.955	227.867	3.9	107.908	117.321
2	3.106	74.55	462.844	2.68	26.804	137.508
3	2.228	40.439	6924.14	4.102	87.477	2056.39
4	3.671	95.627	338.054	1.257	14.386	101.118
5	2.286	22.863	9749.42	2.058	29.062	2954.17
6	3.42	93.21	320.127	1.279	15.324	83.426
7	2.317	33.407	208.629	3.884	85.139	134.108
8	1.455	29.878	3754.15	4.365	78.729	13030.8
9	2.65	89.43	220.33	4.056	108.124	102.57
10	1.759	37.139	12422.6	2.958	57.856	8512.58
11	1.563	35.124	12340.7	3.124	55.124	8417.28
12	2.217	40.124	7012.5	4.12	86.124	2013.78
13	2.317	33.124	200.127	3.9	84.012	112.789
14	3.107	74.128	455.27	2.7	27.124	120.158
15	2.378	22.127	9800.24	2.098	29.012	2801.13
16	1.4	29.12	3600.13	4.427	77.128	14014.6

Figure 6 Stress–strain curve for fabricated configuration 1 of ABS material

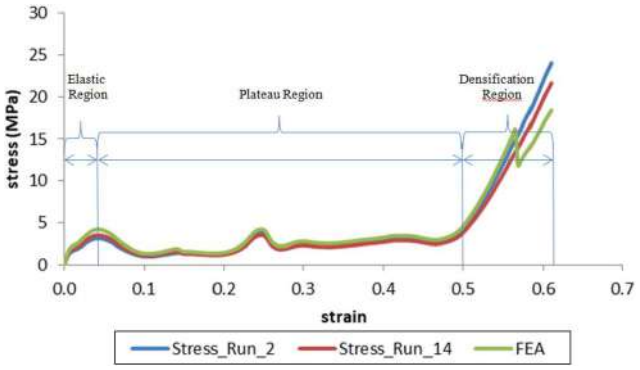

Noticeable differences are observed in the phenomenon of cell collapsing of each configuration. This is the reason for the difference in the properties of configurations. FEA also shows similar stress–strain behavior of configurations. As observed in FEA, stress concentration is indicated at the interaction of vertical and inclined cell walls. Appendix 3 shows a comparison of experimental and FEA deformations of auxetic structures.

The variation in the stress–strain curve is owing to the difference in resistive force exerted by cell-walls. In all configurations, inclined and vertical walls resist external load together and combined deformation mode is observed which is characterized by buckling of vertical walls and bending of inclined walls. When the compressive load is applied to the structure, vertical cell walls behave like end-loaded columns. As the load on the wall reaches to the Euler buckling load, wall buckles Equation (3)).

Table 7 Normalized value of Young's modulus of ABS and PLA

Material	ABS			PLA		
Run no.	Young's modulus of structure (A) MPa	Young's modulus of base material MPa	Normalized value (A/B)	Young's modulus of structure (A) MPa	Young's modulus of base material (B) MPa	Normalized value (A/B)
1	85.955	2,200.000	0.039	107.908	3,500.000	0.031
2	74.550	2,200.000	0.034	26.804	3,500.000	0.008
3	40.439	2,200.000	0.018	87.477	3,500.000	0.025
4	95.627	2,200.000	0.043	14.386	3,500.000	0.004
5	22.863	2,200.000	0.010	29.062	3,500.000	0.008
6	93.210	2,200.000	0.042	15.324	3,500.000	0.004
7	33.407	2,200.000	0.015	85.139	3,500.000	0.024
8	29.878	2,200.000	0.014	78.729	3,500.000	0.022
9	89.430	2,200.000	0.041	108.124	3,500.000	0.031
10	37.139	2,200.000	0.017	57.856	3,500.000	0.017
11	35.124	2,200.000	0.016	55.124	3,500.000	0.016
12	40.124	2,200.000	0.018	86.124	3,500.000	0.025
13	33.124	2,200.000	0.015	84.012	3,500.000	0.024
14	74.128	2,200.000	0.034	27.124	3,500.000	0.008
15	22.127	2,200.000	0.010	29.012	3,500.000	0.008
16	29.120	2,200.000	0.013	77.128	3,500.000	0.022

Table 8 Summary of means and standard deviation of responses w.r.t. factors

	Material →	ABS						PLA					
		Compressive strength (MPa)		Compressive stiffness (MPa)		SEA (J/gm)		Compressive strength (MPa)		Compressive stiffness (MPa)		SEA (J/gm)	
Factor	Levels	Mean	SD	Mean	SD	Mean	SD	Mean	SD	Mean	SD	Mean	SD
Re-entrant angle (degree)	20	2.603	0.864	55.188	32.233	3,560.029	4,095.263	2.608	1.149	37.196	24.137	4155.364	5530.578
	40	2.205	0.374	49.343	23.844	4,944.612	5,455.316	*3.756**	0.424	*83.971**	18.333	2683.352	3428.75
Height (mm)	14	2.392	0.697	50.019	26.964	4,520.617	4,751.796	3.193	0.899	56.844	30.86	1291.254	1286.349
	18	2.313	0.902	61.935	31.36	4,152.995	5,291.594	3.171	1.288	64.322	36.274	5547.462	6133.889
Arm length (mm)	5	*2.897**	0.506	*72.429**	25.402	304.156	108.375	2.957	1.177	58.603	41.513	113.625	14.879
	8	1.911	0.408	32.102	7.241	*8,200.485**	3,462.03	3.407	0.983	62.564	23.829	*6725.091**	4965.137
	Total	2.404	0.676	52.265	27.555	4,252.321	4,714.445	3.182	1.073	60.583	32.763	3419.358	4812.596

Notes: *maximum mean value for each response for all levels of all factors; SD – standard deviation

Table 9 ANOVA results: main effect of factors for responses

	ABS						PLA					
	Compressive strength (MPa)		Compressive stiffness (MPa)		SEA (J/gm)		Compressive strength (MPa)		Compressive stiffness (MPa)		SEA (J/gm)	
Factors	F (df = 1)	*p*	F (df = 1)	*p*	F (df = 1)	*p*	F (df = 1)	*p*	F (df = 1)	*p*	F (df = 1)	*p*
Re-entrant angle (degree)	86.67	< 0.05	93.24	< 0.05	2,968.92	< 0.05	1,433.20	< 0.05	9,889.14	< 0.05	16.55	< 0.05
Height (mm)	18.00	< 0.05	1,020.77	< 0.05	61.11	< 0.05	0.5268	< 0.05	252.77	< 0.05	227.37	< 0.05
Arm length (mm)	531.24	< 0.05	4,438.19	< 0.05	96,562.09	< 0.05	219.92	< 0.05	70.93	< 0.05	8,314.87	< 0.05

Table 10 Summary of correlation of response with geometric parameters

Materials	ABS			PLA		
Parameters	Compressive strength	Compressive stiffness	SEA	Compressive strength	Compressive stiffness	SEA
Re-entrant angle	Negative	Negative	Positive	Positive	Positive	Positive
Height	Positive	Positive	Negative	Positive	Positive	Positive
Arm-length	Negative	Negative	Positive	Negative	Negative	Positive

Figure 7 Predicted vs actual compressive strength

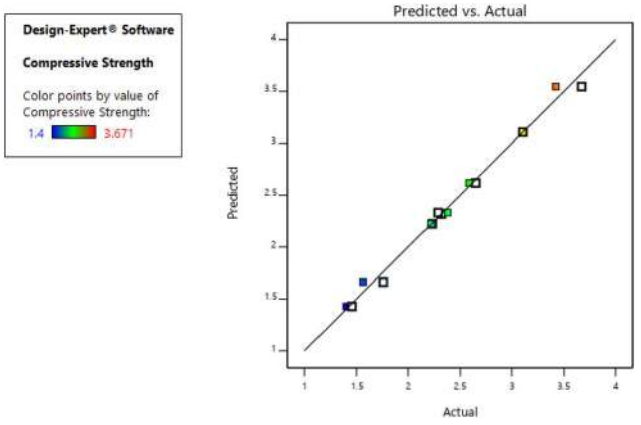

$$P_{cr} = \frac{\pi^2 \times E \times I}{(K \times L)^2} \qquad \text{equation (3)}$$

where,

P_{cr} = Euler's critical load (longitudinal compression load on column);
E = modulus of elasticity of the material;
I = minimum area moment of inertia of the cross-section;
L = unsupported length of column; and
K = column effective length factor.

Rotational stiffness of a node (where three cell walls come into contact) depends upon the degree of the constraint of node rotation caused by inclined cell walls. This results in buckling and bending of vertical cell walls and inclined walls, respectively. The compressive buckling of vertical walls enhances stiffness. It is observed that the base material of the auxetic structure affects deformation behavior and a failure mode.

Compressive strength is stress value at a yield point if yield takes place before 10% strain. In nonappearance of such a yield point, stress at 10% is considered as the compressive strength of the material (Raeisi *et al.*, 2019). Compressive stiffness (Modulus of compression) is the ratio of stress to strain in an elastic region of a material when it is compressed. Cellular materials can be characterized by their energy absorption capacity useful for weight-sensitive applications. The energy

Figure 8 Effect of geometric parameters [(a) re-entrant angle and arm length; (b) arm length and height] on compressive strength of ABS structures

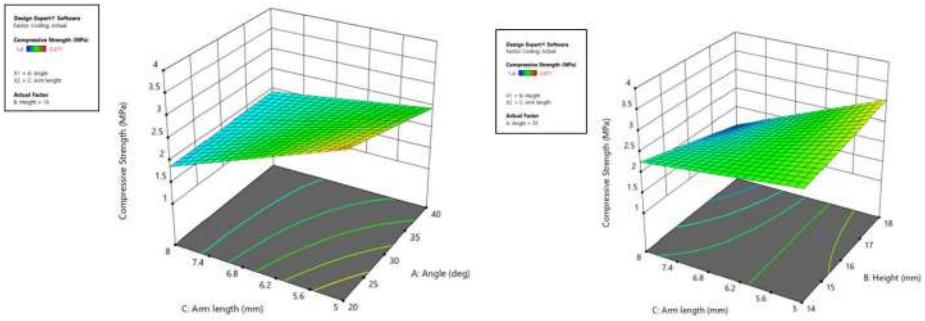

(a) (b)

absorbed during compression is calculated for each configuration by integrating the stress–strain curve [Equation (4)]. SEA of cellular material is given by Equation (5).

$$W = \int_0^{\varepsilon} \sigma(\varepsilon) d\varepsilon \qquad \text{equation (4)}$$

$$\text{SEA} = \frac{\text{W}}{\Delta\rho \times \rho\text{s}} \qquad \text{equation (5)}$$

where

$\Delta\rho$ = relative density of structure; and

ρs = density of bulk material.

Table 7 lists normalized value of Young's modulus of ABS and PLA materials. It is observed that the normalized value of Young's modulus depends on the material of structure. This is owing to the inherent nature of specific material (i.e. ductile and brittle behavior for ABS and PLA material, respectively).

3.1 Deformation of auxetic structures under compressive loading

Structures made up of ABS material have shown ductile and plateau behavior depending upon selected level of geometric parameters. The stress–strain curve of configuration 1 demonstrates steady increase in load corresponding to downward displacement of upper plate of UTM in initial region of load-displacement curve. Initially, load is transferred on third-row of cell walls without much deviation in first and second-row of cell walls because of less cell height of 14 mm. After buckling of third-row cell walls, first-row cell walls buckle in reverse direction owing to resistance offered by second row-cell walls. First-row cell walls are deformed in reverse direction, whereas third-row cell walls are deformed at last stage of loading. The row-by-row deformation of auxetic structure depends upon geometric parameters of unit cell. Deformation of all configurations is shown in Appendix 1.

Structures made up of PLA material have shown brittle behavior depending upon selected level of geometric parameters. Therefore, initial region of load-displacement curve is steeper than the curve obtained for similar configurations of ABS material. For configuration 1 of PLA structure, breakage is observed in first and third-row unit cell walls with less sign of buckling.

In configuration 4 of ABS structure, resistance offered by buckling of second and third-row unit cell walls provides maximum strength and stiffness to the structure. With increase in height and decrease in re-entrant angle, inclined cell walls resist for bending deformation and cell collapses by buckling mode, thus results in higher strength and stiffness of configuration. Similar observations have been reported by Xu *et al.*, 2019. In configuration 7 of PLA structure, maximum value of strength and stiffness is observed with re-entrant angle 20°, height 18 mm and arm-length 8 mm among selected range of geometric parameters.

Figure 9 Effect of geometric parameters [(a) re-entrant angle and height; (b) re-entrant angle and arm length and (c) height and arm length] on compressive strength of PLA structures

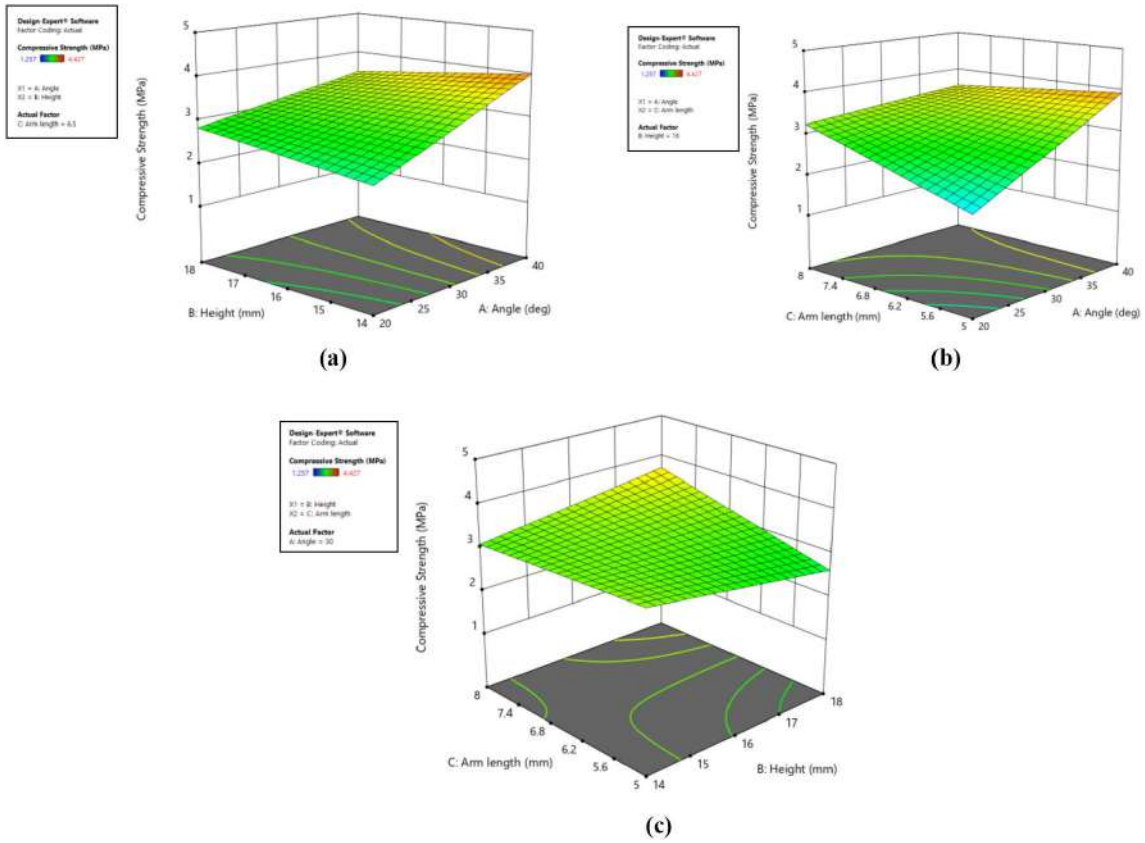

3.2 Influence of geometrical parameters on responses

Summary of means and standard deviation of responses w. r.t. factors are given in Table 8. Analysis of variance (ANOVA) is performed to determine the significance of geometric parameters on responses, namely, compressive strength, stiffness and SEA. Table 9 lists the main effect of factors on responses. From ANOVA, it is found that all three parameters (i.e. re-entrant angle, height and arm length) are significant influencing compressive strength and stiffness, whereas arm length is found most significant parameter influencing SEA of structures made of both the materials (i.e. ABS and PLA). The correlation of responses with geometric parameters of structures is given in Table 10.

For compressive strength interaction of arm length and height, the interaction of re-entrant angle and arm length and interaction of re-entrant angle, height and arm length are found significant for ABS structures. From Figure 7, it is clear that model predictions are in good agreement with experimental results. It is observed from Figure 8 that compressive strength increases with an increase in height and decrease in re-entrant angle and arm length. With an increase in height and decrease in re-entrant angle, inclined cell wall resists for bending deformation and cell walls collapse through buckling mode, which results in higher strength and stiffness. Similar observations are reported by Xu *et al.* (2019). For PLA structures, the interaction of re-entrant angle and height, the interaction of re-entrant angle and arm length and interaction of re-entrant angle, height and arm length are found significant. From Figure 9, it is observed that with an increase in re-entrant angle and height and a decrease in the value of arm length compressive strength of structure increases. Because of inherent brittle nature, PLA structures exhibit different behavior than ABS structures. For less value of the re-entrant angle, bending is not observed in inclined cell walls and these walls fail by brittle fracture. Similar observations are reported by Alomarah *et al.* (2020a, 2020b).

For compressive stiffness, it is found that interaction of re-entrant angle and height, the interaction of re-entrant angle and arm length, interaction of arm length and height and interaction of re-entrant angle, height and arm length are significant for structures made of both the materials. From Figure 10, it is observed that compressive stiffness increases with an increase in height and decrease in re-entrant angle and arm length of unit cells of ABS structures. The reasons for this trend of compressive stiffness are similar to the compressive strength (Xu *et al.*, 2019). As depicted in Figure 11 that for PLA structures, compressive stiffness increases with an increase in re-entrant angle and height and decrease in arm-length of unit cells.

For SEA, the interaction of re-entrant angle and height, interaction of re-entrant angle and arm length, interaction of height and arm length and interaction of re-entrant angle, height and arm length are found significant for ABS structures. From Figure 12, it is observed that SEA increases with an increase in arm length of unit cells. Slight effect of re-entrant angle and height is observed on SEA. For

Figure 10 Effect of geometric parameters [(a) re-entrant angle and height; (b) re-entrant angle and arm length and (c) height and arm length] on compressive stiffness of ABS structures

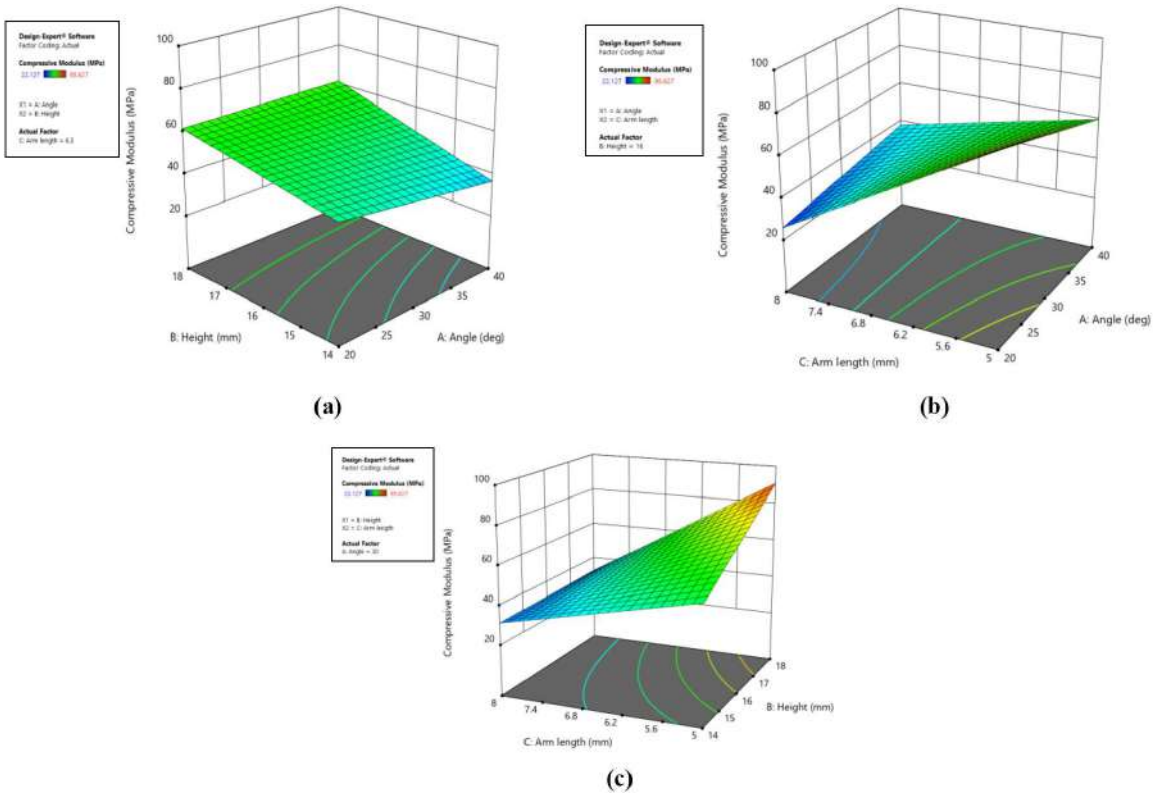

PLA structures, the interaction of re-entrant angle and height and interaction of height and arm length are found significant influencing SEA. From Figure 13, it is clear that SEA increases with an increase in re-entrant angle, height and arm length of unit cells of PLA structures. From stress–strain curves given in Appendix 2, it is observed that less amount of energy is absorbed in elastic deformation, while large amount of energy is absorbed in plastic deformation and fracture. Thus, a larger plateau region means more energy absorption capability of the structure.

Based on ANOVA, regression models of compressive strength, stiffness and SEA of auxetic structures of ABS and PLA materials are developed by using Design-Expert 11 software. All regression models are given in Table 11.

3.3 Optimization of geometric parameters

Optimization of geometric parameters is performed to maximize strength, stiffness and SEA and to minimize weight and time of fabrication of auxetic structures. Gray relational analysis (GRA) technique is used for optimization. This

Figure 11 Effect of geometrical parameters [(a) re-entrant angle and height; (b) re-entrant angle and arm length and (c) height and arm length] on compressive stiffness of PLA structures

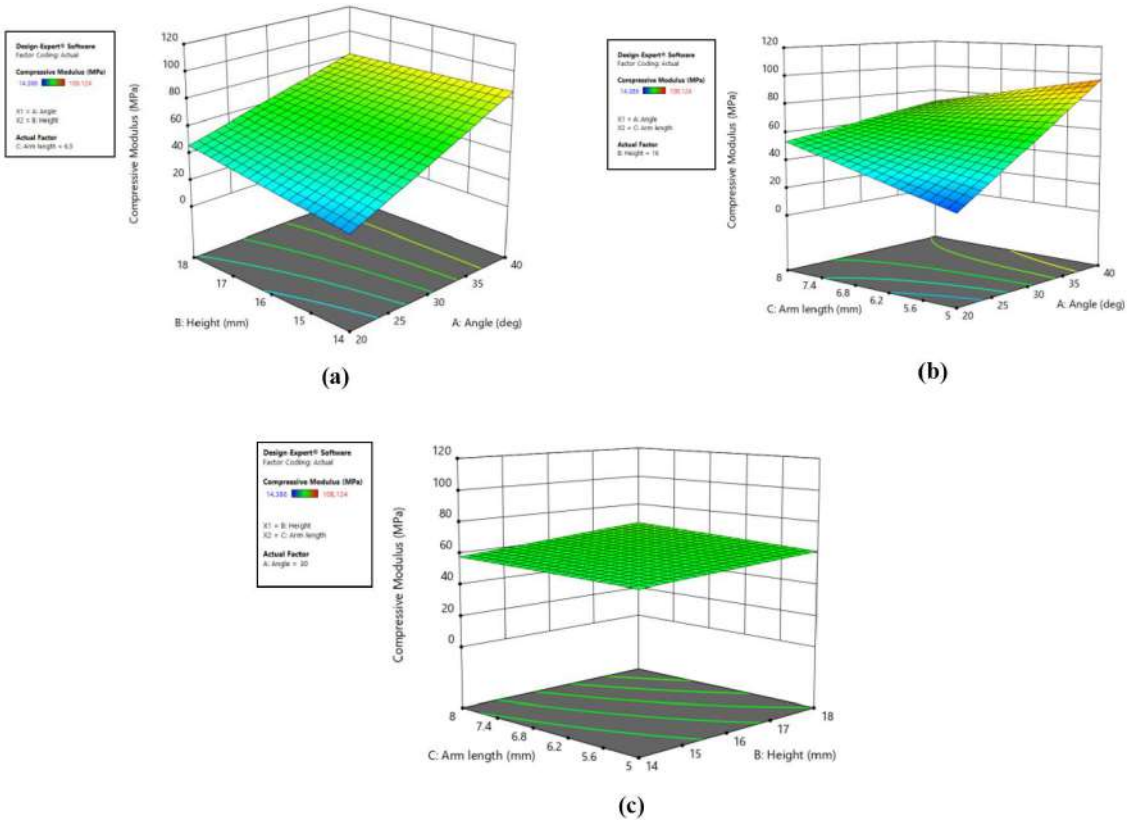

Figure 12 Effect of geometric parameters [(a) re-entrant angle and arm length and (b) height and arm length] on SEA of ABS structures

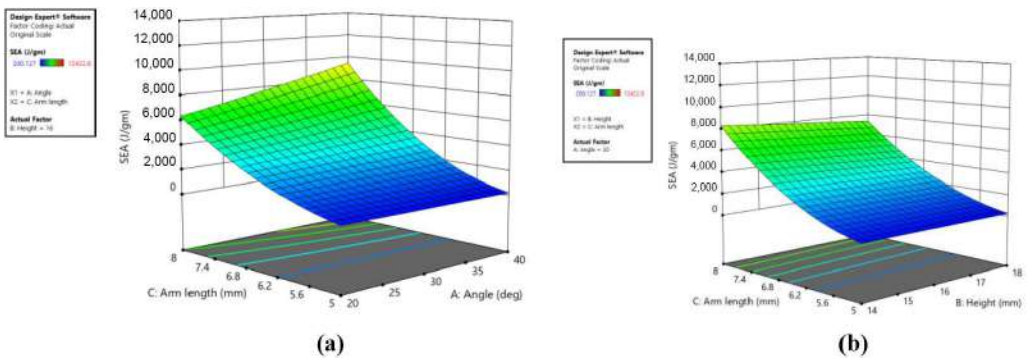

method involves following steps (Sood *et al.*, 2010; Panda *et al.*, 2016) – normalization of responses; computation of deviation sequence; computation of gray relational coefficient; calculation for a gray rational grade (GRG); and finding rank. Calculations of all these steps of GRA for responses of the auxetic structure of ABS and PLA materials are given in Appendix 4 and 5, respectively. It is found that highest GRGs are obtained for following configurations:

For structures of ABS material: configuration 4 with geometric parameters as re-entrant angle 20°, height 18 mm and arm length 5 mm.

For structures of PLA material: configuration 5 with geometric parameters as re-entrant angle 40°, height 14 mm and arm length 5 mm.

3.4 Confirmation tests and comparison of experimental and finite element analysis results

For conducting confirmation tests random settings are selected within the range of geometric parameters. The results are given in Table 12. Optimized settings of factors obtained from GRA are also selected, and the results are listed in Table 13. The deviation percentage is calculated using Equation (6) which is less than 15% therefore acceptable.

$$\text{deviation} \quad \% \quad = \frac{|Predicted\ value - Observed\ value|}{Predicted\ value} \times 100\% \qquad \text{equation 6}$$

Comparison of experimental and FEA results of compressive strength, stiffness and SEA of auxetic structures of ABS and PLA materials are given in Table 14. The deviation percentage

Figure 13 Effect of geometrical parameters [(a) re-entrant angle and arm length (b) height and arm length] on SEA of PLA structures

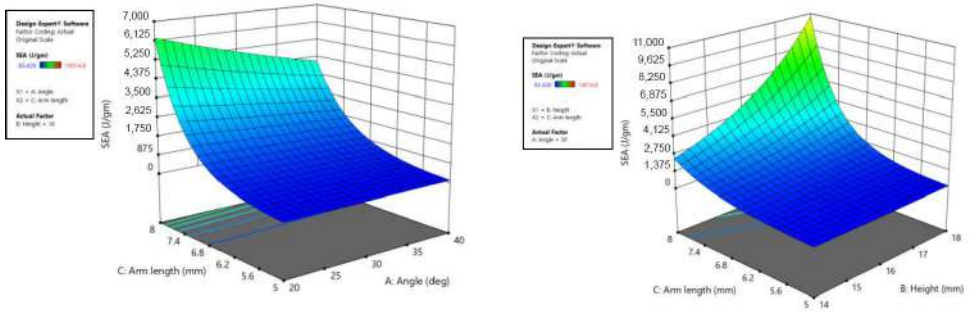

(a) (b)

Notes: (a) Re-entrant angle and arm length; (b) height and arm length on SEA of PLA structures

Table 11 Regression models for strength, stiffness and SEA of auxetic structures

Material →	ABS	PLA
Compressive strength (MPa)	$(-6.34) + (0.07 \times A) + (0.9 \times B) + (1.64 \times C) - (0.01 \times A \times B) - (0.02 \times A \times C) - (0.15 \times B \times C) + (0.002 \times A \times B \times C)$	$(64.52) - (1.70 \times A) - (4.33 \times B) - (10.56 \times C) + (0.12 \times A \times B) + (0.3 \times A \times C) + (0.72 \times B \times C) - (0.02 \times A \times B \times C)$
Compressive stiffness (MPa)	$(539.01) - (26.24 \times A) - (17.08 \times B) - (74.73 \times C) + (1.38 \times A \times B) + (3.64 \times A \times C) + (2.7 \times B \times C) - (0.19 \times A \times B \times C)$	$(1{,}158.18) - (36.82 \times A) - (85.14 \times B) - (204.40 \times C) + (2.84 \times A \times B) + (6.69 \times A \times C) + (14.65 \times B \times C) - (0.48 \times A \times B \times C)$
SEA (J/gm)	$[(-654.83) + (17.74 \times A) + (38.61 \times B) + (141.75 \times C) - (1.24 \times A \times B) - (3.76 \times A \times C) - (8.08 \times B \times C) + (0.26 \times A \times B \times C)]^2$	$\text{antilog}_n((14.16) - (0.12 \times A) - (1.07 \times B) - (1.46 \times C) + (0.01 \times A \times B) + (0.015 \times A \times C) + (0.19 \times B \times C) - (0.001 \times A \times B \times C))$

Notes: A = re-entrant angle (°); B = height (mm); C = arm length (mm)

Table 12 Confirmation tests results for random levels of geometric parameters

		Factors			Compressive strength (MPa)			Compressive modulus (MPa)			SEA (J/gm)		
Material	Experiment no.	Re-entrant angle (°)	Height (mm)	Arm-length (mm)	Predicted	Observed	Deviation (%)	Predicted	Observed	Deviation (%)	Predicted	Observed	Deviation (%)
ABS	1	25	15	6	2.707	3.02	11.563	56.823	60.12	5.802	1812.669	2012.24	11.01
	2	38	17	7	2.068	2.324	12.379	49.357	52.124	5.606	5233.957	5800.41	10.823
PLA	1	25	15	6	2.804	3.214	14.622	43.958	46.127	4.934	378.302	401.29	6.077
	2	38	17	7	3.481	3.612	3.763	74.064	71.127	3.965	1623.059	1806.79	11.32

Table 13 Confirmation tests results for optimized levels of geometric parameters

Material	ABS									PLA								
Confirmation Run no.	Compressive strength (MPa)			Compressive modulus (MPa)			SEA (J/gm)			Compressive strength (MPa)			Compressive modulus (MPa)			SEA (J/gm)		
	Predicted	Observed	Deviation (%)	Predicted	Observed	Deviation (%)	Predicted	Observed	Deviation (%)	Predicted	Observed	Deviation (%)	Predicted	Observed	Deviation (%)	Predicted	Observed	Deviation (%)
1	3.96	3.513	11.288	94.92	85.123	10.321	488.41	417.123	14.596	4.7	4.520	3.830	81.32	73.127	10.075	171.98	161.130	6.309
2	3.96	4.3	8.586	94.92	102.33	7.807	488.41	512.36	4.904	4.7	4.942	5.149	81.32	92.740	14.043	171.98	192.940	12.187
3	3.96	4.620	16.667	94.92	89.124	6.106	488.41	428.13	12.342	4.7	5.123	9.000	81.32	89.780	10.403	171.98	187.130	8.809
Average deviation (%)			12.18			8.078			10.614			5.993			11.507			9.102

Table 14 Comparison of experimental and FEA results

Material	ABS									PLA								
	Compressive strength (MPa)			Compressive stiffness (MPa)			SEA (J/gm)			Compressive strength (MPa)			Compressive stiffness (MPa)			SEA (J/gm)		
Config. no.	Exp.	FEA	Δ	Exp.	FEA	Δ	Exp.	FEA	Δ	Exp.	FEA	Δ	Exp.	FEA	Δ	Exp.	FEA	Δ
1	3.106	2.9	6.632	74.55	70.179	5.863	462.844	422.340	8.751	2.680	2.314	13.657	26.804	30.45	13.602	137.508	150.750	9.630
2	2.286	2.1	8.136	22.863	18.789	17.819	9,749.42	8,824.72	9.485	2.058	2.346	13.994	29.062	26.78	7.852	2,954.17	3,312.76	12.138
3	2.228	2.41	8.169	40.439	34.784	13.984	6,924.14	6,242.78	9.840	4.102	3.842	6.338	87.477	99.42	13.653	2,056.39	2,337.94	13.691
4	3.671	3.21	12.558	95.627	105.670	10.502	338.054	374.740	10.852	1.257	1.413	12.411	14.386	16.14	12.192	101.118	116.130	4.846
5	2.317	2.12	8.502	33.407	28.740	13.970	208.629	239.120	14.615	3.884	3.521	9.346	85.139	90.73	6.567	134.108	143.740	7.182
6	1.759	2.01	14.269	37.139	40.170	8.161	12,422.6	13,899.2	11.886	2.958	3.24	9.533	57.856	62.79	8.528	8,512.58	9,122.94	7.170
7	1.455	1.62	11.340	29.878	26.178	12.384	3,754.15	3,257.870	13.220	4.365	3.923	10.126	78.729	83.75	6.378	13,030.8	13,970.650	7.213
8	2.586	2.31	10.673	85.955	91.270	6.183	227.867	254.74	11.793	3.900	4.32	10.769	107.908	118.760	10.057	117.321	127.290	8.497

Notes: Exp.: experimental value; FEA: FEA value; and Δ: deviation percentage

(Δ) for all structures is found less than 15% which is similar to the results reported by Zhang and Yang (2016).

4. Conclusion

The present paper describes an investigation of FDM fabricated re-entrant auxetic structures of ABS and PLA materials under compressive loading. Followings are the findings of present work.

Re-entrant angle, height and arm-length of unit cells are found significant parameters for strength, stiffness and SEA for structures of ABS and PLA materials.

In case of ABS structures, it is observed that compressive strength and stiffness increases with an increase in height and a decrease in re-entrant angle and arm length of the unit cell. SEA increases with increase in re-entrant angle and arm length and decrease in height.

In case of PLA structures, it is observed that compressive strength and stiffness increases with increase in re-entrant angle and height and decrease in arm length of the unit cell. SEA increases with an increase in re-entrant angle, height and arm length.

It is observed that ABS structures exhibit elastic–plastic collapse behavior, and PLA structures exhibit brittle fracture behavior. Deformation behavior and normalized Young's modulus of auxetic structures is material specific.

Results of FEA are found in good agreement with experimental results. Further, regression models are also developed to predict strength, stiffness and SEA of auxetic structures. Also, optimization of geometric parameters is performed using GRA to maximize strength, stiffness and SEA and minimize weight and time of fabrication. From confirmation experiments, good agreement is found between regression models and confirmation results.

The findings of the present study are useful in fabrication of auxetic structures of maximum strength, stiffness and SEA with minimum weight and time of fabrication. Future research of authors will be focused on studying the strength, stiffness and SEA of auxetic structures of FDM parts under shear and flexural loading. Also, the effect of shrinkage of ABS material on dimensional accuracy and mechanical properties of auxetic structure needs to be investigated.

References

Ahn, S.H., Montero, M., Odell, D., Roundy, S. and Wright, P. K. (2002), "Anisotropic material properties of fused deposition modeling ABS", *Rapid Prototyping Journal*, Vol. 8 No. 4, pp. 248-257.

Alomarah, A., Ruan, D., Xu, S. and Masood, S. (2020b), "Dynamic performance of auxetic structures: experiments and simulation", *Smart Materials and Structures*, Vol. 29 No. 5.

Alomarah, A., Ruan, D., Masood, S., Sbarski, I. and Faisal, B. (2018), "An investigation of in-plane tensile properties of re-entrant chiral auxetic structure", *The International Journal of Advanced Manufacturing Technology*, Vol. 96 Nos 5/8, pp. 2013-2029.

Alomarah, A., Masood, S.H., Sbarski, I., Faisal, B., Gao, Z. and Ruan, D. (2020a), "Compressive properties of 3D printed auxetic structures: experimental and numerical studies", *Virtual and Physical Prototyping*, Vol. 15 No. 1, pp. 1-21.

Al-Rifaie, H. and Sumelka, W. (2019), "The development of a new shock absorbing uniaxial graded auxetic damper (UGAD)", *Materials*, Vol. 12 No. 16, p. 2573.

Araujo, H., Leite, M., Ribeiro, A.R., Deus, A.M., Reis, L. and Vaz, M.F. (2019), "The effect of geometry on the flexural properties of cellular core structures", *Proceedings of the Institution of Mechanical Engineers, Part L: Journal of Materials: Design and Applications*, Vol. 233 No. 3, pp. 338-347.

Attard, D., Farrugia, P.S., Gatt, R. and Grima, J.N. (2020), "Starchirals – a novel class of auxetic hierarchal structures", *International Journal of Mechanical Sciences*, Vol. 179, p. 105631.

Bayar, M.S. and Aziz, Z. (2018), "Rapid prototyping and its role in supporting architectural design process", *Journal of Architectural Engineering*, Vol. 24 No. 3, p. 05018003.

Chen, Y., Li, T., Jia, Z., Scarpa, F., Yao, C.W. and Wang, L. (2018), "3D printed hierarchical honeycombs with shape integrity under large compressive deformations", *Materials and Design*, Vol. 137, pp. 226-234.

Durgun, I. (2015), "Sheet metal forming using FDM rapid prototype tool", *Rapid Prototyping Journal*, Vol. 21 No. 4, pp. 412-422.

El-Katatny, I., Masood, S.H. and Morsi, Y.S. (2010), "Error analysis of FDM fabricated medical replicas", *Rapid Prototyping Journal*, Vol. 16 No. 1, pp. 36-43.

Elipe, J.C.Á. and Lantada, A.D. (2012), "Comparative study of auxetic geometries by means of computer-aided design and engineering", *Smart Materials and Structures*, Vol. 21 No. 10, p. 105004.

Francesconi, L., Baldi, A., Dominguez, G. and Taylor, M. (2019b), "An investigation of the enhanced fatigue performance of low-porosity auxetic metamaterials", *Experimental Mechanics*, Vol. 60 No. 1, pp. 1-15.

Francesconi, L., Baldi, A., Liang, X., Aymerich, F. and Taylor, M. (2019a), "Variable Poisson's ratio materials for globally stable static and dynamic compression resistance", *Extreme Mechanics Letters*, Vol. 26, pp. 1-7.

Gao, Q., Tan, C.A., Hulbert, G. and Wang, L. (2020), "Geometrically nonlinear mechanical properties of auxetic double-V microstructures with negative Poisson's ratio", *European Journal of Mechanics-A/Solids*, Vol. 80, p. 103933.

Garcia-Garcia, R. and Gonzalez-Palacios, M.A. (2018), "Method for the geometric modeling and rapid prototyping of involute bevel gears", *The International Journal of Advanced Manufacturing Technology*, Vol. 98 Nos 1/4, pp. 645-656.

Gibson, L.J. and Ashby, M.F. (1999), *Cellular Solids: structure and Properties*, Cambridge university press.

Ingrole, A., Hao, A. and Liang, R. (2017), "Design and modeling of auxetic and hybrid honeycomb structures for in-plane property enhancement", *Materials & Design*, Vol. 117, pp. 72-83.

Korpela, J., Kokkari, A., Korhonen, H., Malin, M., Närhi, T. and Seppälä, J. (2013), "Biodegradable and bioactive porous scaffold structures prepared using fused deposition modeling", *Journal of Biomedical Materials Research Part B: Applied Biomaterials*, Vol. 101B No. 4, pp. 610-619.

Lam, C.X.F., Mo, X.M., Teoh, S.H. and Hutmacher, D.W. (2002), "Scaffold development using 3D printing with a starch-based polymer", *Materials Science and Engineering: C*, Vol. 20 Nos 1/2, pp. 49-56.

Lee, W., Jeong, Y., Yoo, J., Huh, H., Park, S.J., Park, S.H. and Yoon, J. (2019), "Effect of auxetic structures on crash behavior of cylindrical tube", *Composite Structures*, Vol. 208, pp. 836-846.

Li, X., Lu, Z., Yang, Z. and Yang, C. (2018a), "Anisotropic in-plane mechanical behavior of square honeycombs under off-axis loading", *Materials & Design*, Vol. 158, pp. 88-97.

Li, X., Wang, Q., Yang, Z. and Lu, Z. (2019), "Novel auxetic structures with enhanced mechanical properties", *Extreme Mechanics Letters*, Vol. 27, pp. 59-65.

Li, T., Chen, Y., Hu, X., Li, Y. and Wang, L. (2018b), "Exploiting negative Poisson's ratio to design 3D-printed composites with enhanced mechanical properties", *Materials & Design*, Vol. 142, pp. 247-258.

McCaw, J.C. and Cuan-Urquizo, E. (2020), "Mechanical characterization of 3D printed, non-planar lattice structures under quasi-static cyclic loading", *Rapid Prototyping Journal*, Vol. 26 No. 4, pp. 707-717, doi: 10.1108/RPJ-06-2019-0163.

Meier, M., Tan, K.H., Lim, M.K. and Chung, L. (2018), "Unlocking innovation in the sport industry through additive manufacturing", *Business Process Management Journal*, Vol. 25 No. 3.

Negis, E. (2009), "A short history and applications of 3D printing technologies in Turkey", in *US-Turkey Workshop on Rapid Technologies*, Vol. 24, pp. 23-30.

Okwuosa, T.C., Stefaniak, D., Arafat, B., Isreb, A., Wan, K.W. and Alhnan, M.A. (2016), "A lower temperature FDM 3D printing for the manufacture of patient-specific immediate release tablets", *Pharmaceutical Research*, Vol. 33 No. 11, pp. 2704-2712.

Panda, B., Leite, M., Biswal, B.B., Niu, X. and Garg, A. (2018), "Experimental and numerical modeling of mechanical properties of 3D printed honeycomb structures", *Measurement*, Vol. 116, pp. 495-506.

Panda, A., Sahoo, A. and Rout, R. (2016), "Multi-attribute decision making parametric optimization and modeling in hard turning using ceramic insert through gray relational analysis: a case study", *Decision Science Letters*, Vol. 5 No. 4, pp. 581-592.

Raeisi, S., Tapkir, P., Ansari, F. and Tovar, A. (2019), "Design of a hybrid honeycomb unit cell with enhanced in-Plane mechanical properties (no. 2019-01-0710)", SAE Technical Paper.

Saxena, K.K. Das, R. and Calius, E.P. (2017), "3D printable multimaterial cellular auxetics with tunable stiffness", arXiv preprint arXiv:1707.04486.

Scarpa, F., Panayiotou, P. and Tomlinson, G. (2000), "Numerical and experimental uniaxial loading on in-plane auxetic honeycombs", *The Journal of Strain Analysis for Engineering Design*, Vol. 35 No. 5, pp. 383-388.

Scarpa, F., Blain, S., Lew, T., Perrott, D., Ruzzene, M. and Yates, J.R. (2007), "Elastic buckling of hexagonal chiral cell honeycombs", *Composites Part A: Applied Science and Manufacturing*, Vol. 38 No. 2, pp. 280-289.

Sood, A.K., Ohdar, R.K. and Mahapatra, S.S. (2010), "Parametric appraisal of fused deposition modeling process using the gray Taguchi method", *Proceedings of the Institution of Mechanical Engineers, Part B: Journal of Engineering Manufacture*, Vol. 224 No. 1, pp. 135-145.

Surjadi, J.U., Gao, L., Du, H., Li, X., Xiong, X., Fang, N.X. and Lu, Y. (2019), "Mechanical metamaterials and their engineering applications", *Advanced Engineering Materials*, Vol. 21 No. 3, p. 1800864.

Wang, Z., Li, Z. and Xiong, W. (2019), "Numerical study on three-point bending behavior of honeycomb sandwich with ceramic tile", *Composites Part B: Engineering*, Vol. 167, pp. 63-70.

Xu, M., Xu, Z., Zhang, Z., Lei, H., Bai, Y. and Fang, D. (2019), "Mechanical properties and energy absorption capability of AuxHex structure under in-plane compression: theoretical and experimental studies", *International Journal of Mechanical Sciences*, Vol. 159, pp. 43-57.

Xu, J., Wu, Y., Wang, L., Li, J., Yang, Y., Tian, Y., Gong, Z., Zhang, P., Nutt, S. and Yin, S. (2018), "Compressive properties of hollow lattice truss reinforced honeycombs (honeytubes) by additive manufacturing: patterning and tube alignment effects", *Materials & Design*, Vol. 156, pp. 446-457.

Yang, C., Vora, H.D. and Chang, Y. (2018), "Behavior of auxetic structures under compression and impact forces", *Smart Materials and Structures*, Vol. 27 No. 2, p. 025012.

Yang, L., Harrysson, O., West, H. and Cormier, D. (2015), "Mechanical properties of 3D re-entrant honeycomb auxetic structures realized via additive manufacturing", *International Journal of Solids and Structures*, Vol. 69-70, pp. 475-490.

Yu, X., Zhou, J., Liang, H., Jiang, Z. and Wu, L. (2018), "Mechanical metamaterials associated with stiffness, rigidity and compressibility: a brief review", *Progress in Materials Science*, Vol. 94, pp. 114-173.

Zhang, X. and Yang, D. (2016), "Mechanical properties of auxetic cellular material consisting of re-entrant hexagonal honeycombs", *Materials*, Vol. 9 No. 11, p. 900.

Corresponding author

Shailendra Kumar can be contacted at: skbudhwar@gmail.com

Appendix 1

Figure A1 Deformation of auxetic structures under compressive loading at nominal strain (ε) of 0.15

Configuration Number	ABS	PLA
1		
2		
3		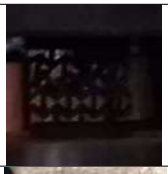
4		
5		
6		
7		
8		

Appendix 2

Figure A2 Stress-strain curves of ABS and PLA structures

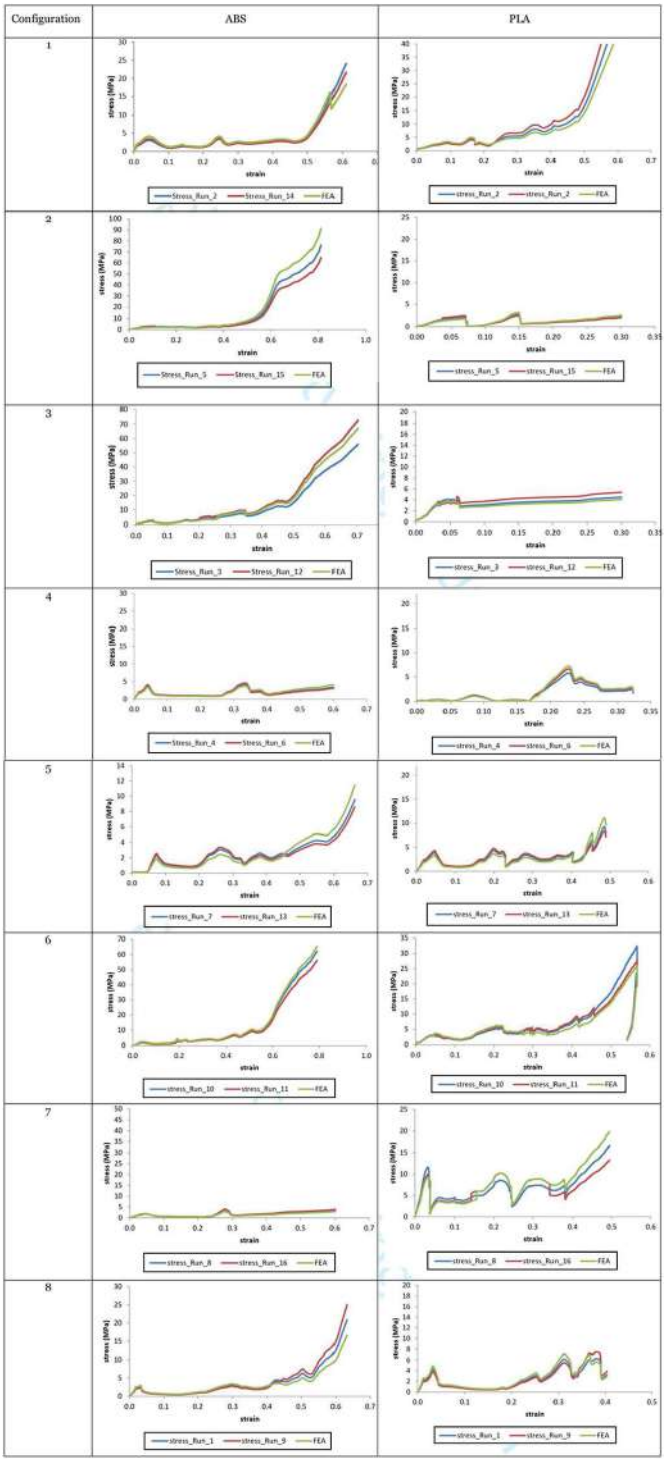

Appendix 3

Figure A3 Comparison of Experimental and FEA deformation under compressive load on auxetic structures at 15% strain

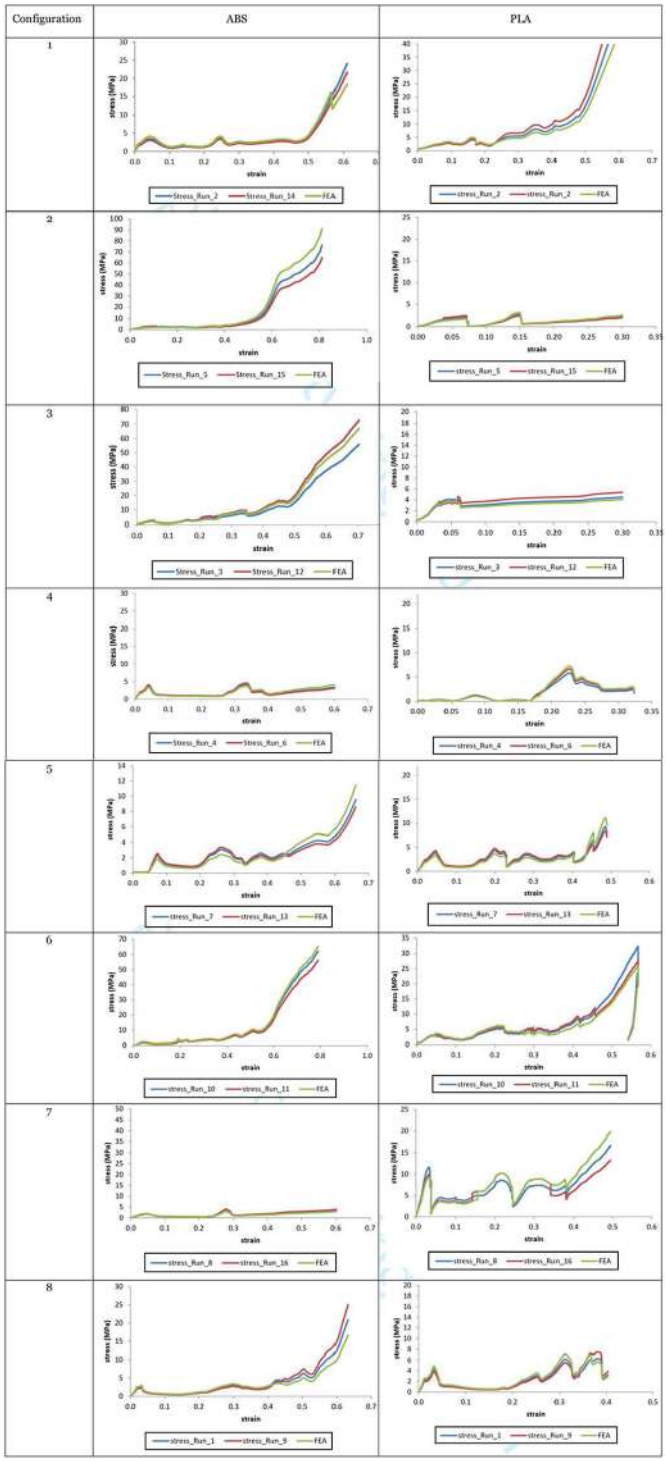

Appendix 4

Table A1 GRA calculations for ABS structures

Run no.	Compressive Strength (MPa)	Compressive Stiffness (MPa)	SEA (J/gm)	Weight (gm)	Time (minutes)	Comp. strength	Comp. Stiffness	SEA	Weight	Time	Comp. strength
						Step 1: Normalization of responses					Step 2: Deviation Sequence
1	2.586	85.955	227.87	33.19	308	0.51	0.867	0.002	0.859	0.803	0.49
2	3.106	74.55	462.84	37.63	289	0.745	0.71	0.021	0.727	0.928	0.255
3	*2.23*	*40.44*	*6924*	41.39	304	0.349	0.242	0.55	0.615	0.829	0.651
4	*3.67*	*95.63*	*338.1*	43.29	310	1	1	0.011	0.559	0.789	0
5	*2.29*	*22.86*	*9749*	55.96	402	0.375	0	0.781	0.184	0.184	0.625
6	3.651	94.123	320.13	43.29	310	0.991	0.979	0.01	0.559	0.789	0.009
7	*2.32*	*33.41*	*208.6*	28.42	278	0.389	0.145	0.001	1	1	0.611
8	*1.46*	*29.88*	*3754*	62.15	430	0	0.096	0.291	0	0	1
9	*2.65*	*89.43*	*220.3*	33.19	308	0.539	0.915	0.002	0.859	0.803	0.461
10	*1.76*	*37.14*	*12423*	62.15	380	0.137	0.196	1	0	0.329	0.863
11	1.743	36.127	12341	62.15	380	0.13	0.182	0.993	0	0.329	0.87
12	2.22	41.324	7012.5	41.39	304	0.345	0.254	0.557	0.615	0.829	0.655
13	2.307	34.123	200.13	28.42	278	0.384	0.155	0	1	1	0.616
14	*3.1*	*75.12*	*455.3*	37.63	289	0.743	0.718	0.021	0.727	0.928	0.257
15	2.28	23.125	9800.2	55.96	402	0.372	0.004	0.785	0.184	0.184	0.628
16	1.467	30.125	3600.1	62.15	430	0.005	0.1	0.278	0	0	0.995

(*continued*)

Table A1

	Step 2: Deviation Sequence				Step 3: Grey relational coefficient					Step 4: Grey relation grade	Step 5
Run no.	Comp. Stiffness	SEA	Weight	Time	Comp. strength	Comp. Stiffness	SEA	Weight	Time	GRG	Rank
1	0.133	0.998	0.141	0.197	0.505	0.79	0.334	0.78	0.717	0.625	8
2	0.29	0.979	0.273	0.072	0.662	0.633	0.338	0.647	0.874	0.631	5
3	0.758	0.45	0.385	0.171	0.434	0.397	0.526	0.565	0.745	0.534	10
4	0	0.989	0.441	0.211	1	1	0.336	0.531	0.704	0.714	1
5	1	0.219	0.816	0.816	0.444	0.333	0.696	0.38	0.38	0.447	14
6	0.021	0.99	0.441	0.211	0.982	0.96	0.336	0.531	0.704	0.703	2
7	0.855	0.999	0	0	0.45	0.369	0.333	1	1	0.631	7
8	0.904	0.709	1	1	0.333	0.356	0.413	0.333	0.333	0.354	15
9	0.085	0.998	0.141	0.197	0.52	0.855	0.334	0.78	0.717	0.641	3
10	0.804	0	1	0.671	0.367	0.383	1	0.333	0.427	0.502	11
11	0.818	0.007	1	0.671	0.365	0.379	0.987	0.333	0.427	0.498	12
12	0.746	0.443	0.385	0.171	0.433	0.401	0.53	0.565	0.745	0.535	9
13	0.845	1	0	0	0.448	0.372	0.333	1	1	0.631	6
14	0.282	0.979	0.273	0.072	0.66	0.64	0.338	0.647	0.874	0.632	4
15	0.996	0.215	0.816	0.816	0.443	0.334	0.7	0.38	0.38	0.447	13
16	0.9	0.722	1	1	0.335	0.357	0.409	0.333	0.333	0.354	16

Appendix 5

Table A2

Run no.	Compressive Strength (MPa)	Compressive Stiffness (MPa)	SEA (J/gm)	Weight (gm)	Time (minutes)	Step 1: Normalization of responses					Step 2: Deviation Sequence	
						Comp. strength	Comp. Stiffness	SEA	Weight	Time	Comp. strength	Comp. Stiffness
1	3.9	107.91	117.32	33.19	308	0.834	0.998	0.002	0.859	0.803	0.166	0.002
2	2.68	26.804	137.51	37.63	289	0.449	0.132	0.004	0.727	0.928	0.551	0.868
3	*4.1*	*87.48*	*2056*	41.39	304	0.897	0.78	0.142	0.615	0.829	0.103	0.22
4	*1.26*	*14.39*	*101.1*	43.29	310	0	0	0.001	0.559	0.789	1	1
5	*2.06*	*29.06*	*2954*	55.96	402	0.253	0.157	0.206	0.184	0.184	0.747	0.843
6	1.324	15.324	83.426	43.29	310	0.021	0.01	0	0.559	0.789	0.979	0.99
7	*3.88*	*85.14*	*134.1*	28.42	278	0.829	0.755	0.004	1	1	0.171	0.245
8	*4.37*	*78.73*	*13031*	62.15	430	0.98	0.686	0.929	0	0	0.02	0.314
9	*4.2*	*108.1*	*102.6*	33.19	308	0.928	1	0.001	0.859	0.803	0.072	0
10	*2.96*	*57.86*	*8513*	62.15	380	0.537	0.464	0.605	0	0.329	0.463	0.536
11	3.124	55.124	8417.3	62.15	380	0.589	0.435	0.598	0	0.329	0.411	0.565
12	4.274	86.124	2013.8	41.39	304	0.952	0.765	0.139	0.615	0.829	0.048	0.235
13	3.942	84.012	112.79	28.42	278	0.847	0.743	0.002	1	1	0.153	0.257
14	*2.78*	*27.12*	*120.2*	37.63	289	0.482	0.136	0.003	0.727	0.928	0.518	0.864
15	2.137	29.012	2801.1	55.96	402	0.278	0.156	0.195	0.184	0.184	0.722	0.844
16	4.427	77.128	14015	62.15	430	1	0.669	1	0	0	0	0.331

(*continued*)

Table A2

	Step 2: Deviation Sequence				Step 3: Grey relational coefficient				Step 4: Grey relation grade	Step 5
Run no.	SEA	Weight	Time	Comp. strength	Comp. modulus	SEA	Weight	Time	GRG	Rank
1	0.998	0.141	0.197	0.75	0.995	0.334	0.78	0.717	0.715	4
2	0.996	0.273	0.072	0.476	0.366	0.334	0.647	0.874	0.539	10
3	0.858	0.385	0.171	0.83	0.694	0.368	0.565	0.745	0.64	7
4	0.999	0.441	0.211	0.333	0.333	0.334	0.531	0.704	0.447	14
5	0.794	0.816	0.816	0.401	0.372	0.386	0.38	0.38	0.384	16
6	1	0.441	0.211	0.338	0.336	0.333	0.531	0.704	0.448	13
7	0.996	0	0	0.745	0.671	0.334	1	1	0.75	2
8	0.071	1	1	0.962	0.615	0.876	0.333	0.333	0.624	8
9	0.999	0.141	0.197	0.875	1	0.334	0.78	0.717	0.741	3
10	0.395	1	0.671	0.519	0.483	0.559	0.333	0.427	0.464	12
11	0.402	1	0.671	0.549	0.469	0.554	0.333	0.427	0.467	11
12	0.861	0.385	0.171	0.912	0.681	0.367	0.565	0.745	0.654	5
13	0.998	0	0	0.766	0.66	0.334	1	1	0.752	1
14	0.997	0.273	0.072	0.491	0.367	0.334	0.647	0.874	0.542	9
15	0.805	0.816	0.816	0.409	0.372	0.383	0.38	0.38	0.385	15
16	0	1	1	1	0.602	1	0.333	0.333	0.654	6